

1 **This manuscript has been submitted for publication in GEOSCIENCE FRONTIERS. Please**  
2 **note that, despite undergoing peer review, the manuscript has yet to be formally accepted for**  
3 **publication. Subsequent versions of this manuscript may have slightly different content.**  
4 **If accepted, the final version of this manuscript will be available via the ‘Peer-reviewed**  
5 **Publication DOI’ link on the right-hand side of this webpage. Please feel free to contact any of**  
6 **the authors; we welcome feedback.**

7  
8 **Title** - Eclogites and basement terrane tectonics in the northern arm of the Grenville orogen, NW  
9 Scotland

10 **Authors** - A. Bird<sup>1</sup>, M. Thirlwall<sup>2</sup>, R.A. Strachan<sup>3</sup>, I. L. Millar<sup>4</sup>, E.D. Dempsey<sup>1</sup>, K. Hardman<sup>1</sup>

11 **Affiliations** - 1. School of Environmental Sciences, University of Hull, Cottingham Road, Hull,  
12 HU6 7RX

13 2. Department of Earth Sciences, Royal Holloway University of London, Egham, Surrey, TW20  
14 0EX

15 3. School of the Environment, Geography and Geosciences, University of Portsmouth, Burnaby Rd,  
16 Portsmouth, PO1 3QL.

17 4. Geochronology and Tracers, British Geological Survey, Keyworth, Nottinghamshire, NG12 5GG

18  
19  
20

# Eclogites and basement terrane tectonics in the northern arm of the Grenville orogen, NW Scotland

A. Bird<sup>1</sup>, M. Thirlwall<sup>2</sup>, R.A. Strachan<sup>3</sup>, I. L. Millar<sup>4</sup>, E.D. Dempsey<sup>1</sup>, K. Hardman<sup>1</sup>

1. School of Environmental Sciences, University of Hull, Cottingham Road, Hull, HU6 7RX

2. Department of Earth Sciences, Royal Holloway University of London, Egham, Surrey, TW20  
0EX

3. School of the Environment, Geography and Geosciences, University of Portsmouth, Burnaby Rd,  
Portsmouth, PO1 3QL.

4. Geochronology and Tracers, British Geological Survey, Keyworth, Nottinghamshire, NG12 5GG

## ABSTRACT

The presence of eclogites within continental crust is a key indicator of collisional orogenesis and they have been used worldwide to assist in the delineation of ancient collisional sutures. Eclogites within the Eastern Glenelg basement inlier of the Northern Highland Terrane (NHT) have been re-dated in order to provide more accurate constraints on the timing of collision within the northern arm of the Grenville Orogen. The eclogites yield dates of c.1200 Ma which are interpreted to record the onset of convergence, and the NHT as a whole is thought to represent the lower plate in successive 1200-1000 Ma collision events. The Eastern Glenelg basement inlier is viewed as a fragment of the leading edge of the NHT basement that was partially subducted along a suture and then obducted back up the subduction channel. Differences in ages of igneous protoliths and intrusive histories (Storey et al., 2010; Strachan et al., 2020b), and metamorphic events (this paper) between the NHT basement and the Laurentian foreland, suggests that they were separate crustal blocks until after c. 1600 Ma. We therefore suggest that: 1) the NHT represents a fragment of Archean-Paleoproterozoic crust that was reworked within the c. 1600-1700 Ga Labradorian-Gothian belt, although whether it was derived from Laurentia or Baltica (Strachan et al., 2020b) is uncertain (Fig. 3), and 2) amalgamation of the NHT with the Laurentian foreland did not occur until the terminal stages of the Grenville collision at c. 1000 Ma.

## HIGHLIGHTS

1200 Ma eclogites from the Scottish Northern Highlands

Scottish Northern Highlands reworked within Labradorian-Gothian belt (1.6-1.7Ga)

50 Scottish Northern Highland eclogites record onset of Rodinia amalgamation

51 Scottish Northern Highlands and Laurentian foreland amalgamation occurred after 1Ga

## 52 **1.1 INTRODUCTION**

53 The presence of eclogites within continental crust is a key indicator of collisional orogenesis. This  
54 is because they typically represent a low thermal gradient ( $<350\text{ }^{\circ}\text{C GPa}^{-1}$ ) which is essential for  
55 high pressure/medium-low temperature metamorphism. Such thermal gradients are far lower than  
56 the geotherm expected within normal thickness continental crust, and imply orogenesis and in  
57 particular deep subduction (e.g. Brown, 2007). Eclogites have therefore been used worldwide to  
58 assist in the delineation of collisional sutures (e.g. Trans-Hudson orogen, Weller, 2017; Himalaya,  
59 O'Brian, 2018), and can therefore be used to unravel the complex collages of accreted terranes that  
60 make up substantial parts of many orogens. Key issues include whether or not accreted terranes can  
61 be linked to the foreland of an orogen or are instead allochthonous and derived from a colliding  
62 craton or intervening ocean. Tectonic analysis of deeply eroded Precambrian gneiss complexes is  
63 particularly difficult as faunal controls are absent and palaeomagnetic constraints are often poor.  
64 As an example, there has been much debate concerning the assembly of Rodinia and specifically the  
65 tectonic setting of the c.1.0 Ga Grenville and Sveconorwegian orogens. In one interpretation, they  
66 are different parts of the same collisional belt that resulted from the collision of Laurentia,  
67 Amazonia and Baltica (Fig 1d; Bingen et al., 2021, Cawood and Pisarevsky, 2017). Alternatively,  
68 following its rifting from Laurentia at or after c. 1265 Ma (Fig 1c), Baltica always remained  
69 outboard and separate from the Amazonia-Laurentia collision, and the Sveconorwegian orogeny  
70 was accretionary in nature (Slagstad et al., 2019, 2013; Slagstad and Kirkland, 2017). In this paper  
71 we present new isotopic data from reworked basement gneiss complexes in NW Scotland and  
72 consider the implications for Mesoproterozoic tectonics in this sector of Rodinia.

73 The Northern Highland Terrane (NHT) of the Lower Palaeozoic Caledonide orogen in NW  
74 Scotland (Fig. 2 inset) is dominated by the Neoproterozoic Moine Supergroup, and inliers of largely  
75 orthogneissic basement that have been correlated with the Archean-Paleoproterozoic Lewisian  
76 Gneiss Complex of the Laurentian foreland to the west (Fig 2a & b; Friend et al., 2008). This  
77 correlation is largely based on the lithological similarities between the mainly TTG orthogneisses of  
78 the Lewisian Gneiss Complex and the Inliers, and comparable Neoproterozoic and Paleoproterozoic U-  
79 Pb zircon protolith ages (Fig. 3). Alternatively, it has been suggested that the basement inliers  
80 represent a fragment of Baltican basement that was transferred to the Scottish margin of Laurentia  
81 following Grenville-age collision and subsequent Ediacaran rifting of Rodinia to form the Iapetus

82 Ocean (Strachan et al., 2020a). Further support for the latter hypothesis is provided by a  
83 multidimensional scaling analysis of published U-Pb zircon data, including some from Scandinavia,  
84 and which shows that there are generally two groups of Inliers, one group with a more Laurentian  
85 (Lewisian Gneiss Complex) affinity and one with potentially more of a Baltican affinity (Fig 3).

86 Eclogites that have yielded Sm-Nd mineral-whole rock isochrons of c. 1.1-1.0 Ga occur within the  
87 Eastern Glenelg basement inlier along the western margin of the Scottish Caledonides (Fig 2b;  
88 Sanders et al., 1984) and provide critical evidence for high-pressure Grenville metamorphism in this  
89 segment of Rodinia, although its wider significance has remained uncertain. The Eastern Glenelg  
90 eclogites occur close to the Caledonian Moine Thrust which defines the easterly-dipping boundary  
91 between the Laurentian foreland and the NHT and has been interpreted as a reworked Grenville  
92 front (Fig. 2b; Sanders et al., 1984). Here we report the results of isotopic dating from the Eastern  
93 Glenelg inlier and also, for the purposes of comparison, from the Borgie inlier further north (Fig 2a)  
94 that establish that 1) the NHT basement was affected by a high-grade metamorphic event at c. 1680-  
95 1630 Ma, which is largely absent on the Laurentian foreland, 2) eclogite-facies metamorphism  
96 occurred at c. 1180 Ma, at least c. 100 myr older than thought previously. We propose a tectonic  
97 model for the amalgamation of basement terranes and eclogite formation in this sector of the North  
98 Atlantic, within a northern arm of the Grenville belt.

## 99 **2.1 GEOLOGICAL SETTING OF THE EASTERN GLENELG ECLOGITES AND THE** 100 **NHT BASEMENT**

101 The Neoproterozoic and Paleoproterozoic basement inliers within the NHT are dominated by tonalitic  
102 to dioritic hornblende gneisses with minor supracrustal layers, and occur either as fold cores or  
103 thrust slices (Friend et al., 2008; Strachan et al., 2020b, 2020a, 2010). The inliers have been  
104 strongly reworked at amphibolite facies during Neoproterozoic and Ordovician-Silurian  
105 (Caledonian) orogenic events, but in areas of low tectonic strain and minimal retrogression preserve  
106 evidence of older and higher grades of metamorphism. The Eastern Glenelg inlier incorporates units  
107 of garnet-kyanite pelite that are often closely associated with mafic and felsic rocks which contain  
108 pods and lenses of eclogite. Ultrabasic rocks are also present as olivine websterites +/- garnet. The  
109 pelites and the eclogite protoliths likely formed part of a supracrustal sequence that accumulated at  
110 c. 2000 Ma on pre-existing orthogneisses of probable Neoproterozoic protolith age (Storey et al., 2010  
111 and Supplementary Data 2). The eclogites are typically composed of garnet + omphacite + rutile +  
112 quartz (Sanders, 1989). Pressure-temperature estimations obtained from various lithologies,  
113 including the eclogites, indicate peak metamorphic conditions of c. 20 kbar and 730-750°C,

114 consistent with burial to depths of c. 70 km. Two samples of eclogite yielded Sm-Nd garnet-  
115 clinopyroxene-whole rock isochron ages of  $1082 \pm 24$  Ma and  $1010 \pm 13$  Ma (Sanders et al., 1984).  
116 For the purposes of comparison, we also consider the Neoproterozoic Borgie basement inlier (Fig. 2a)  
117 that occupies a similar structural setting 150 km further north (Fig 2a). The inlier is exposed in the  
118 core of a composite antiform (Strachan et al., 2020a) and consists mainly of banded felsic to  
119 intermediate, amphibolite facies orthogneisses (Friend et al., 2008). Mafic and ultramafic pods and  
120 sheets contain relic garnet-clinopyroxene metamorphic assemblages indicative of upper amphibolite  
121 to granulite facies metamorphism (Holdsworth et al., 2001).

### 122 3.1 SAMPLE DESCRIPTIONS

123 Three samples were collected from the supracrustal sequence within the Eastern Unit of the  
124 Glenelg-Attadale, one from a garnet-kyanite-phengitic white mica pelite and two from eclogitic  
125 pods. The garnet-kyanite-phengitic pelite (AB07-12, NG 9049 2330, Fig. 2) shows a strong  
126 schistosity (Rawson et al., 2001) and is associated with marble, that is interfolded with  
127 orthogneisses. It contains mauve coloured garnet porphyroblasts up to 5 mm in size, biotite,  
128 plagioclase, quartz, white mica, chlorite, rutile, sillimanite and kyanite (the kyanite is not seen in  
129 hand specimen). The white mica in this sample has been studied by Rawson (2002) who found it to  
130 be phengitic in composition indicating that they may be relicts of the eclogite facies. The biotite,  
131 white mica and quartz define the schistose fabric which is wrapping the garnets. Kyanite is not  
132 common and is always associated with biotite. The garnets have inclusions of quartz, mica,  
133 opaques and quite large rounded zircons ( $70\mu\text{m}$ ). Zircons are also present within biotites where  
134 they have pleochroic halos. Sillimanite (fibrolite) is present in very small needles which cluster at  
135 the rims of plagioclase grains.

136 The eclogites (AB07-09, NG 8411 2142; AB07-10, NG 8603 2343, Fig. 2) were collected from  
137 mafic pods cut by a network of quartzo-feldspathic veins (“streaks”) that range in size from  
138 millimetre to tens of centimetre scale. According to Sanders (1989), the veins/ streaks formed  
139 during eclogite facies metamorphism. There are also hydrated layers of amphibolitised material  
140 cutting through the eclogite pods. The rocks are strongly tectonised with a dominant early fabric  
141 and has prominent lineations. In thin section, AB07-09 has a coarse granoblastic polygonal texture  
142 (up to 4 mm). It comprises garnet, omphacite, rutile and quartz, with veins/ streaks which contain  
143 quartz, plagioclase and kyanite. The kyanite sometimes forms asymmetric fish, indicating non-  
144 coaxial shearing within the streaks. Garnets are up to 4 mm in size, extremely plentiful and quite  
145 inclusion-free with some alteration to amphibole around the rims. Inclusions, where present,

146 consist of rutile, omphacite, quartz, zircon and opaques which sometimes define linear trails.  
147 Omphacite grains occur with symplectites of diopside and plagioclase and are replaced around their  
148 rims by hornblende. Rutile has been replaced round the rims by ilmenite. The veins of  
149 amphibolitisation are much greener as more hornblende occurs and more symplectites are also  
150 present. AB07-10 is very similar to AB07-09 but is more retrogressed, in places, rutile intergrowths  
151 and inclusions have almost entirely been replaced by framboidal rims of titanite. The matrix is  
152 dominated by symplectitic intergrowths which are probably of diopside, plagioclase and quartz, and  
153 a blue-green amphibole is replacing the omphacite.

154 A sample from the Borgie garnet-clinopyroxene orthogneiss (AB-07-18) was obtained from a  
155 massive cm-scale mafic pod within the Borgie Inlier. The sample is structureless and dominated by  
156 garnet and clinopyroxene, which have undergone minor replacement by retrogressive hornblende.  
157 The garnets are euhedral to subhedral in shape often with some amphibole around the edges, and  
158 contain inclusions of clinopyroxene, rutile and opaques. The amphibole typically is replacing the  
159 clinopyroxene around grain rims and sometimes along cleavage planes. The plagioclase is multiple  
160 twinned and has inclusions of clinopyroxene.

#### 161 **4.1 ANALYTICAL METHODS**

162 Trace element maps of garnets were obtained from all samples by laser ablation inductively coupled  
163 plasma mass spectrometry (LA-ICPMS) at the University of Hull. Based on the zoning patterns  
164 shown by the LA-ICPMS data, all of the Lu-Hf and Sm-Nd ages should be meaningful (Fig. 4). The  
165 Lu shows some zoning in AB07-09 and AB07-10 (Fig. 4 A and E), suggesting that the Lu-Hf dates  
166 are likely to relate to garnet growth or close to peak metamorphism. AB07-12 and AB07-18 do not  
167 show zoning. As AB07-18 records granulite facies metamorphism, this likely relates to the high  
168 temperature nature of this sample, and thus the date probably represents post-peak metamorphism  
169 but could still be close to peak. AB07-12 is from a sample which is likely not to have recorded such  
170 high temperatures, suggesting that this date might relate to later diffusion/cooling during  
171 exhumation or resetting during later metamorphic events. In all cases, apart from AB07-18, the Sm  
172 and Nd maps show less zoning than the Lu maps, suggesting that the Sm-Nd ages are more likely  
173 than the Lu-Hf ages to reflect cooling or resetting. U-Pb zircon and Rb-Sr white mica and biotite  
174 ages were obtained from the pelite sample for comparative purposes with the Lu-Hf and Sm-Nd  
175 data. Full details of samples, analytical procedures and all maps produced are provided in  
176 Supplementary Data 1 and all isotopic and geochemical results are in Supplementary Data 2.

#### 177 **5.1 RESULTS**

178 Samples from the Eastern Glenelg pelite (sample AB07-12) scatter around a Lu-Hf garnet-whole  
179 rock errorchron date of  $1089 \pm 76$  Ma, (MSWD=680, Fig 5A). The four two-point Lu-Hf garnet-  
180 whole rock ages range from 1039-1162 Ma, and have a strong positive correlation with Lu/Hf ratio  
181 and Lu content, and a negative correlation with Hf ( $r^2 = 0.9985$ ). Measured Hf contents in the  
182 dissolved garnet fractions range from 1 to 1.6 ppm, substantially higher than the 0.1ppm measured  
183 in the garnet by LA-ICP-MS, suggesting that Hf-bearing inclusions such as zircon were dissolved.  
184 Combining grt fractions 3 and 4 along with the fused whole rock gives a 3-point Lu-Hf isochron  
185 date of  $1039.6 \pm 3.7$  Ma (MSWD = 0.1, Fig 5A). Sm-Nd garnet and whole rock data lie around an  
186 errorchron corresponding to an age of  $913 \pm 19$  Ma, while low Sm/Nd garnet fractions 3 and 4 yield  
187 higher two-point garnet-WR dates of  $941 \pm 6$  Ma and  $948 \pm 7$  Ma respectively, in contrast to the  
188 Lu-Hf system, where they yield lower 2-point dates and lie on a three-point isochron of  $943 \pm 11.4$   
189 Ma (MSWD = 4.1). Model Nd and Hf dates are around 1.9-2.0 Ga. This sample also provides a  
190 zircon U-Pb Concordia age of  $1648.8 \pm 5.5$  Ma (MSWD=9.1, n=24, all grains less than 15%  
191 discordant, Fig. 5C). These zircons would have had  $^{176}\text{Hf}/^{177}\text{Hf}$  of  $\sim 0.28160$  if they grew from the  
192 whole rock at 1650 Ma, not low enough to account for the low Lu-Hf ages of garnet fractions B, C  
193 and D if they had been present as inclusions in the garnet. Only zircon inclusions with  $^{176}\text{Hf}/^{177}\text{Hf} <$   
194  $\sim 0.2810$  can account for the low Lu-Hf ages, and these would have to be Archean, for which there  
195 is little evidence in the zircon population. The sample also gives a two-point Rb-Sr white mica-  
196 whole rock date of  $1042 \pm 13$  Ma and a biotite-WR date of  $418.7 \pm 1.3$  Ma (Fig. 5D).

197 The Borgie garnet-clinopyroxene orthogneiss sample (AB-07-18) yielded a four-point Lu-  
198 Hf garnet-whole rock-fused whole rock age of  $1634 \pm 9$  Ma (MSWD 0.6) (Fig 5A), and a three-  
199 point Sm-Nd garnet-whole rock date of  $1462 \pm 3.0$  Ma, MSWD 3.8 (Fig. 5B). The Lu-Hf isochron  
200 age is close to Lu-Hf model age for the sample and slightly younger than the Nd model age (1.9  
201 Ga).

202 Samples from eclogite AB-07-09 scatter around a six-point Lu-Hf garnet-whole rock  
203 errorchron date of  $1173 \pm 37$  Ma (MSWD=230, Fig 5A), and around a Sm-Nd errorchron date of  
204  $988 \pm 26$  Ma (MSWD=59). Individual garnet-WR two-point Lu-Hf ages are higher at higher  
205  $^{176}\text{Lu}/^{177}\text{Hf}$  and higher Lu, from  $1138 \pm 5$  Ma to  $1218 \pm 4$  Ma, but unlike AB07-12, do not  
206 correspond to Hf content, which is much lower in this sample (0.19-0.28ppm), suggesting minimal  
207 dissolution of Hf-bearing inclusions. The correlation likely indicates mixing between unidentified  
208 growth zones, implying core growth at  $>1218$  Ma (see Supplementary Data 2 for graphs and more  
209 information), suggesting that if there is mixing present between different growth zones, these zones  
210 are close together in age and are therefore likely to have grown throughout the same orogenic event.

211 This is consistent with the LA-ICP-MS traverse across a garnet from this rock, which has two Lu  
212 concentration peaks at around 1.2 and 0.8 ppm, comparable to the maximum 1.22 ppm and  
213 minimum 0.67 ppm Lu measured on the dissolved garnet fractions. Individual Sm-Nd two-point  
214 ages range from  $949 \pm 8$  to  $988 \pm 4$  Ma, and have a strong positive correlation with  $^{147}\text{Sm}/^{144}\text{Nd}$  and a  
215 strong negative correlation with Nd content. The garnet fraction that yielded the 988 Ma age has Sm  
216 and Nd contents of 2.4 and 1.9 ppm respectively, very comparable to those measured by LA-ICP-  
217 MS ( $2.3 \pm 1.1$  ppm and  $1.4 \pm 0.8$  ppm respectively, 2sd, N=280), those with lower ages have  
218 significantly greater Nd (3.8 ppm) suggesting contamination with other phases. The garnets from  
219 this sample lie on a 4-point isochron of  $1007 \pm 14.2$  (MSWD=9.6). The Hf model age for AB07/09  
220 is around 1.4 Ga.

221 Samples from eclogite AB-07-10 scatter around a six-point Lu-Hf garnet-whole rock errorchron of  
222  $1170 \pm 21$  Ma (MSWD=92, Fig 5A), and a Sm-Nd garnet-whole rock errorchron of  $945 \pm 31$  Ma  
223 (MSWD=44, Fig 5B). Garnet fractions 2, 3 and 4 lie on a  $1159.0 \pm 5.3$  Ma Lu-Hf isochron with the  
224 fused WR (MSWD 4.4), but fraction 1 has a higher two-point age ( $1202 \pm 5$  Ma) coupled with much  
225 higher Lu/Hf, Lu and lower Hf, similar to AB07-09. For both eclogites, measured ID Hf  
226 concentrations in garnets are little higher than in situ Hf contents, suggesting that zircons have little  
227 influence on the observed Lu-Hf ages. Since Lu contents measured by LA-ICP-MS peak in the  
228 garnet cores, it is likely that the older two-point ages for AB07-09 and AB07-10 sample most  
229 closely constrain core growth, and these are very similar between the two eclogites, at  $1202 \pm 5$  and  
230  $1218 \pm 4$  Ma.

## 231 **6.1 DISCUSSION**

### 232 **6.1.1 Significance of the new isotopic ages**

233 The Lu-Hf garnet and U-Pb zircon ages of 1635 Ma obtained from the Borgie inlier and the Eastern  
234 Glenelg pelite broadly compare to Lu-Hf garnet ages obtained from an eclogite ( $1667 \pm 6$  Ma) and a  
235 high-pressure granulite ( $1718 \pm 6$  Ma) within the Western Glenelg inlier (Storey et al., 2010).  
236 Friend et al. (2008) also reported a U-Pb zircon lower intercept age of c. 1600 Ma from the Borgie  
237 inlier, which was interpreted to represent a significant isotopic disturbance with further ~1600-1750  
238 Ma dates recorded in the Rigibill, Loch Shin, Rosemarkie, Farr and Swordly inliers (Fig. 3).  
239 Together, the data suggest that a c. 1600-1700 Ma high-grade metamorphic event that at least  
240 locally attained eclogite-facies is a defining feature of the NHT basement. In contrast, within the  
241 Lewisian Gneiss Complex of the Laurentian foreland the youngest high-grade (= granulite facies)  
242 metamorphic event occurred at c. 1870 Ma (Baba, 1998, Fig 5D), with subsequent events at c.



243 1750-1650 Ma restricted to amphibolite-facies reworking and minor magmatism and anatexis  
244 (Kinny et al., 2005; Wheeler et al., 2010). Whether the c. 1460 Ma Sm-Nd age obtained from the  
245 Borgie inlier reflects cooling or a younger metamorphic event is uncertain.

246 The new Lu-Hf garnet ages of c. 1202 Ma and c. 1218 Ma obtained from the Eastern  
247 Glenelg eclogites are c. 100 Ma older than the published Sm-Nd ages of c. 1010-1080 Ma (Sanders  
248 et al., 1984). Lu-Hf dating is considered to be the more reliable technique for recording peak  
249 metamorphism, as it is believed to have a higher closure temperature (e.g. Scherer et al., 2000;  
250 Anczkiewicz et al., 2007), and thus the new ages are thought to more closely date eclogite-facies  
251 metamorphism. In addition, the LA ICPMS trace element garnet maps show that Lu concentrations  
252 are higher within the garnet cores whereas Sm and Nd are more homogenous throughout the garnets  
253 as a whole (Supplementary Data 1). The Lu-Hf date from the Eastern Unit pelite (1039 Ma) is  
254 younger than the eclogite dates, perhaps reflecting a bigger influence from dissolved Hf-rich  
255 phases. The new Sm-Nd garnet and Rb-Sr white mica ages range from c. 1042 Ma to 943 Ma and  
256 probably result from two separate metamorphic events (Fig 5D). The two older ages of c. 1042 Ma  
257 (AB07-12, Rb-Sr white mica) and c. 988 Ma (AB07-09, Sm-Nd garnet) are plausibly related to  
258 terminal Grenville metamorphism as they are similar to the U-Pb zircon age of  $995 \pm 8$  Ma reported  
259 from the Eastern Glenelg eclogites and attributed to amphibolite facies retrogression (Brewer et al.,  
260 2003). The younger Sm-Nd garnet ages of c. 935 Ma (AB07-10) and c. 943 Ma (AB07-12) are  
261 closer to the age of the oldest metamorphic event known to affect the Moine metasedimentary cover  
262 of the NHT at c. 950-940 Ma, which has been assigned to the onset of Valhalla accretionary  
263 orogenesis around the Laurentian margin of Rodinia (Cawood et al. 2010; Bird et al., 2018, Fig  
264 5D).

### 265 **6.1.2 A new tectonic model for eclogites and basement terrane amalgamation in NW** 266 **Scotland**

267 Published c. 1010-1080 Ma Sm-Nd ages for the Eastern Glenelg eclogites were initially interpreted  
268 to show that they formed during the Grenville orogeny (Sanders et al., 1984). However, since the  
269 publication of these ages there have been major advances in the understanding of this orogen in its  
270 type area of NE Canada, which is now known to comprise a number of autochthonous and  
271 allochthonous tectonic units and to have evolved over 265 myr (Rivers 2008 and references  
272 therein). The outboard late Mesoproterozoic (<1300 Ma) arc terranes of the Composite Arc and the  
273 Frontenac-Adirondack belts record, respectively accretionary orogenic events at 1245-1225 Ma  
274 (Elzevirian) and 1190-1140 Ma (Shawinigan), prior to their accretion to Laurentia at the start of the

275 main 1090-1020 Ma (Ottawan) and 1010-980 Ma (Rigolet) collisional phases of the orogeny  
276 (Rivers 2008). The new ages obtained for the Eastern Glenelg eclogites are thus over 100 myr older  
277 than the onset of the main Grenville continental collision. They are temporally coincident with the  
278 Shawinigan orogenic event but the geological context is very different as in Scotland the eclogites  
279 are not associated with the accretion of juvenile arc material. In summary, there are no  
280 straightforward correlations between the Grenville belt in its type area and the Eastern Glenelg  
281 eclogites.

282 Any alternative tectonic model needs to account for: 1) the formation and location of the  
283 eclogites at c. 1200 Ma, and 2) the differences in metamorphic history between the NHT and the  
284 Laurentian foreland. A possible solution is found in tectonic models that propose a c. 90° rotation of  
285 Baltica relative to Laurentia between c. 1265 and 1000 Ma (Cawood and Pisarevsky, 2006). Prior to  
286 c. 1265 Ma, present-day west Norway faced south (present-day coordinates) and an open ocean, but  
287 by c. 1000 Ma it was juxtaposed against the sector of the Laurentian margin that contained Rockall  
288 Bank and the Laurentian foreland (Fig 1). One effect of this rotation was to open a new oceanic  
289 tract, the Asgard Sea, along the edge of Rodinia (Cawood et al., 2010). Further inboard, the rotation  
290 can only have been accomplished by a corresponding loss of oceanic lithosphere between Laurentia  
291 and Baltica as the latter rotated. Whether this was achieved by oroclinal bending of the subduction  
292 zone developed along the southern Laurentia-Baltica margin or the development of new subduction  
293 zones is uncertain, but the net effect was likely to ‘sweep up’ a series of marginal basins, magmatic  
294 arcs and microcontinental fragments as the two cratons converged, ultimately to collide by c. 1000  
295 Ma. We interpret the Eastern Glenelg eclogites to record the onset of convergence and the NHT as a  
296 whole to represent the upper plate in successive 1200-1000 Ma collision events. The Eastern  
297 Glenelg basement inlier is viewed as a fragment of the leading edge of the NHT basement that was  
298 partially subducted along a suture and then obducted back up the subduction channel. Differences in  
299 the ages of igneous protoliths and intrusive histories (Storey et al. 2010; Strachan et al. 2020a), and  
300 metamorphic events (this paper) between the NHT basement and the Laurentian foreland, suggests  
301 that they were separate crustal blocks until after c. 1600 Ma. We therefore suggest that: 1) the NHT  
302 represents a fragment of Archean-Paleoproterozoic crust that was reworked within the c. 1600-1700  
303 Ma Labradorian-Gothian belt, although whether it was derived from Laurentia or Baltica (Strachan  
304 et al. 2020a) is uncertain (Fig. 3), and 2) amalgamation of the NHT with the Laurentian foreland did  
305 not occur until the terminal stages of the Grenville collision at c. 1000 Ma.

306 The c. 1000 Ma suture between the Laurentian foreland and the NHT is presumably located  
307 some distance (c. 100 kms?) further east in the footwall of the Caledonian Moine Thrust. None the

308 less, various geological features of the foreland could be interpreted as ‘far-field’ responses to  
309 Grenville terrane amalgamation. These include: 1) the c. 1180 Ma Stoer Group (Parnell et al., 2011)  
310 which has been interpreted as a rift basin deposit (Stewart, 2002) but nothing precludes it  
311 representing the fill of a foreland basin, and 2) Rb-Sr biotite ages of c. 1150 Ma in the northern  
312 Outer Hebrides (Cliff and Rex, 1995), and  $^{40}\text{Ar}/^{39}\text{Ar}$  ages obtained from pseudotachylyte veins in  
313 the Outer Hebrides (c. 1200-1300 Ma) and on the Scottish mainland (c. 910-1019 Ma; Sherlock et  
314 al., 2008, 2009).

315 Most reconstructions of the Grenville-Sveconorwegian orogen extrapolate the northern  
316 ‘front’ of the orogen eastwards from Canada to lie just north of the Annagh Gneiss Complex of NW  
317 Ireland, and thence further east to link with its continuation in west Norway (Fig 6; e.g. Buchan et  
318 al., 2000). This does not explain the 1200-1000 Ma events in NW Scotland, which was probably  
319 located c. 500-700 km further north once late Caledonian strike-slip displacement along the Great  
320 Glen Fault is restored (Fig 6). Our proposed tectonic model resolves this issue by explaining these  
321 events as the result of Laurentia-Baltica collision and hence provides evidence for the putative  
322 northern arm of the Grenville orogen favoured by Gee et al. (2016). Grenville-aged metamorphism  
323 at c. 1050 Ma has been recorded in the Shetland Islands (Walker et al. 2020) although there is no  
324 reason to suppose that this arm of the orogen extended any further north.

## 325 REFERENCES CITED

- 326 Anczkiewicz, R., Viola, G., Müntener, O., Thirlwall, M.F., Villa, I.M., Quong, N.Q., 2007.  
327 Structure and shearing conditions in the Day Nui Con Voi massif: Implications for the  
328 evolution of the Red River shear zone in northern Vietnam. *Tectonics* 26, n/a-n/a.  
329 <https://doi.org/10.1029/2006TC001972>
- 330 Baba, S., 1998. Proterozoic anticlockwise P-T path of the Lewisian Complex of South Harris, Outer  
331 Hebrides, NW Scotland. *J. Metamorph. Geol.* 16, 819–841. <https://doi.org/10.1111/j.1525-1314.1998.00163.x>
- 333 Baker, T.R., Prave, A.R., Spencer, C.J., 2019. 1.99 Ga mafic magmatism in the Rona terrane of the  
334 Lewisian Gneiss Complex in Scotland. *Precambrian Res.* 329, 224–231.  
335 <https://doi.org/10.1016/j.precamres.2018.12.027>
- 336 Bergh, S.G., Corfu, F., Priyatkina, N., Kullerud, K., Myhre, P.I., 2015. Multiple post-Svecofennian  
337 1750-1560Ma pegmatite dykes in Archaean-Palaeoproterozoic rocks of the West Troms  
338 Basement Complex, North Norway: Geological significance and regional implications.

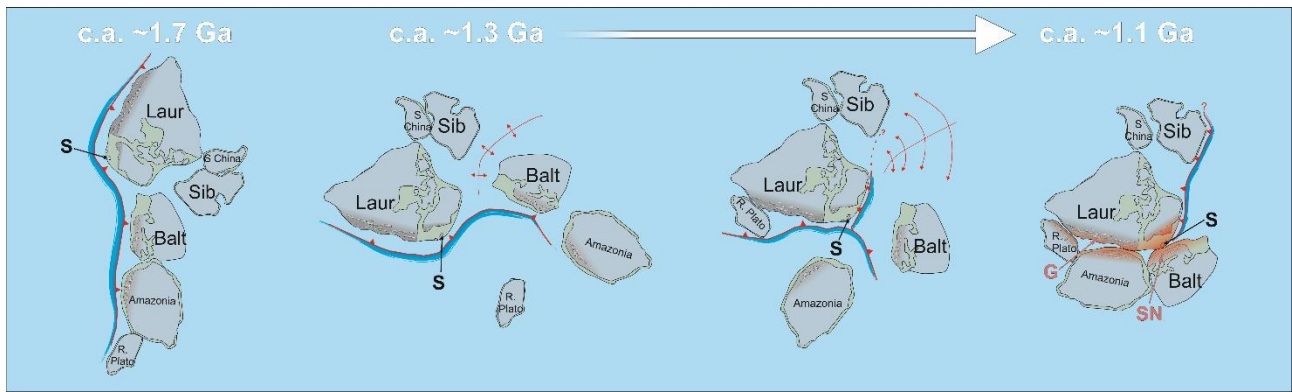
- 339 Precambrian Res. 266, 425–439. <https://doi.org/10.1016/j.precamres.2015.05.035>
- 340 Bingen, B., Viola, G., Möller, C., Vander Auwera, J., Laurent, A., Yi, K., 2021. The  
341 Sveconorwegian orogeny. *Gondwana Res.* 90, 273–313.  
342 <https://doi.org/10.1016/j.gr.2020.10.014>
- 343 Bird, A.F., Thirlwall, M.F., Strachan, R.A., Manning, C.J., Holloway, R., Oex, E.T.W., 2013. Lu –  
344 Hf and Sm – Nd dating of metamorphic garnet : evidence for multiple accretion events during  
345 the Caledonian orogeny in Scotland 170, 301–317. <https://doi.org/10.1144/jgs2012-083.Lu>
- 346 Brown, M., 2007. Metamorphic conditions in orogenic belts: A record of secular change. *Int. Geol.*  
347 *Rev.* 49, 193–234. <https://doi.org/10.2747/0020-6814.49.3.193>
- 348 Buchan, K.L., Mertanen, S., Park, R.G., Pesonen, L.J., Abrahamsen, N., Bylund, G., 2000.  
349 Comparing the drift of Laurentia and Baltica in the Proterozoic : the importance of key  
350 palaeomagnetic poles 319, 167–198.
- 351 Cawood, P.A., Pisarevsky, S.A., 2017. Laurentia-Baltica-Amaozonia relations during Rodinia  
352 assembly. *Precambrian Res.* 292, 386–397. <https://doi.org/10.1016/j.precamres.2017.01.031>
- 353 Corfu, F., Heaman, L.M., Rogers, G., 1994. Polymetamorphic evolution of the Lewisian complex,  
354 NW Scotland, as recorded by U-Pb isotopic compositions of zircon, titanite and rutile. *Contrib.*  
355 *to Mineral. Petrol.* 117, 215–228. <https://doi.org/10.1007/BF00310864>
- 356 Crowley, Q.G., Key, R., Noble, S.R., 2015. High-precision U-Pb dating of complex zircon from the  
357 Lewisian Gneiss Complex of Scotland using an incremental CA-ID-TIMS approach.  
358 *Gondwana Res.* 27, 1381–1391. <https://doi.org/10.1016/j.gr.2014.04.001>
- 359 Daly, J.S., 1996. Pre-Caledonian History of the Annagh Gneiss Complex North-Western Ireland ,  
360 and Correlation with Laurentia-Baltica Author ( s ): J . Stephen Daly Source : Irish Journal of  
361 Earth Sciences , 1996 , Vol . 15 ( 1996 ) , pp . 5-18 Published by : Royal Irish Aca. Irish J.  
362 Earth Sci. 15, 5–18.
- 363 Daly, J.S., 1991. A precise U-Pb zircon age for the Inishtrahull syenitic gneiss, County Donegal,  
364 Ireland. *J. Geol. Soc. London.* 148, 639–642. <https://doi.org/10.1144/gsjgs.148.4.0639>
- 365 Davies, J.H.F.L., Heaman, L.M., 2014. New U-Pb baddeleyite and zircon ages for the Scourie dyke  
366 swarm: A long-lived large igneous province with implications for the Paleoproterozoic  
367 evolution of NW Scotland. *Precambrian Res.* 249, 180–198.  
368 <https://doi.org/10.1016/j.precamres.2014.05.007>

- 369 Fischer, S., Prave, A.R., Johnson, T.E., Cawood, P.A., Hawkesworth, C.J., Horstwood, M.S.A.,  
370 EIMF, 2021. Using zircon in mafic migmatites to disentangle complex high-grade gneiss  
371 terrains – Terrane spotting in the Lewisian complex, NW Scotland. *Precambrian Res.* 355,  
372 106074. <https://doi.org/10.1016/j.precamres.2020.106074>
- 373 Friend, C.R.L., Strachan, R. a., Kinny, P.D., 2008. U-Pb zircon dating of basement inliers within  
374 the Moine Supergroup, Scottish Caledonides: implications of Archaean protolith ages. *J. Geol.*  
375 *Soc. London.* 165, 807–815. <https://doi.org/10.1144/0016-76492007-125>
- 376 Holdsworth, R.E., Strachan, R.A. & Alsop, G.I. 2001. *Geology of the Tongue District*. Memoir of the  
377 British Geological Survey, HMSO.
- 378 Love, G.J., Kinny, P.D., Friend, C.R.L., 2004. Timing of magmatism and metamorphism in the  
379 Gruinard Bay area of the Lewisian Gneiss Complex: Comparisons with the Assynt Terrane and  
380 implications for terrane accretion. *Contrib. to Mineral. Petrol.* 146, 620–636.  
381 <https://doi.org/10.1007/s00410-003-0519-1>
- 382 Mendum, J.R., Noble, S.R., 2010. Mid-Devonian sinistral transpressional movements on the Great  
383 Glen Fault: The rise of the Rosemarkie Inlier and the Acadian event in Scotland. *Geol. Soc.*  
384 *Spec. Publ.* 335, 161–187. <https://doi.org/10.1144/SP335.8>
- 385 Rawson, J.R., Carswell, D.A., Smallwood, D., 2001. Garnet-bearing olivine-websterite within the  
386 Eastern Glenelg Lewisian of the Glenelg Inlier, NW Highlands. *Scottish J. Geol.* 37, 27–34.  
387 <https://doi.org/10.1144/sjg37010027>
- 388 Sanders, I.S., 1989. Phase relations and P-T conditions for eclogite-facies rocks at Glenelg, north-  
389 west Scotland. *Geol. Soc. London, Spec. Publ.* 43, 513–517.  
390 <https://doi.org/10.1144/GSL.SP.1989.043.01.49>
- 391 Sanders, I.S., van Calstreren, P.W.C., Hawkesworth, C.J., 1984. A Grenville Sm–Nd age for the  
392 Glenelg eclogite in north-west Scotland. *Lett. to Nat.* 312.
- 393 Scherer, E.E., Cameron, K.L., Blichert-Toft, J., 2000. Lu – Hf garnet geochronology : Closure  
394 temperature relative to the Sm – Nd system and the effects of trace mineral inclusions.  
395 *Geochim. Cosmochim. Acta* 64, 3413–3432.
- 396 Slagstad, T., Kirkland, C.L., 2017. The use of detrital zircon data in terrane analysis: A nonunique  
397 answer to provenance and tectonostratigraphic position in the Scandinavian Caledonides.  
398 *Lithosphere* 9, 1002–1011. <https://doi.org/10.1130/L663.1>

- 399 Slagstad, T., Kulakov, E., Kirkland, C.L., Roberts, N.M.W., Ganerød, M., 2019. Breaking the  
400 Grenville–Sveconorwegian link in Rodinia reconstructions. *Terra Nov.* 31, 430–437.  
401 <https://doi.org/10.1111/ter.12406>
- 402 Slagstad, T., Roberts, N.M.W., Marker, M., Røhr, T.S., Schiellerup, H., 2013. A non-collisional,  
403 accretionary Sveconorwegian orogen. *Terra Nov.* 25, 30–37. <https://doi.org/10.1111/ter.12001>
- 404 Smit, M.A., Scherer, E.E., Mezger, K., 2013. Lu-Hf and Sm-Nd garnet geochronology:  
405 Chronometric closure and implications for dating petrological processes. *Earth Planet. Sci.*  
406 *Lett.* 381, 222–233. <https://doi.org/10.1016/j.epsl.2013.08.046>
- 407 Stewart, A.D., 2002. The Later Proterozoic Torridonian Rocks of Scotland: Their Sedimentary,  
408 Geochemistry and Origin. Geological Society of London, Issue 24 of Memoir.
- 409 Storey, C.D., Brewer, T.S., Anczkiewicz, R., Parrish, R.R., Thirlwall, M.F., 2010. Multiple high-  
410 pressure metamorphic events and crustal telescoping in the NW Highlands of Scotland. *J.*  
411 *Geol. Soc. London.* 167, 455–468. <https://doi.org/10.1144/0016-76492009-024>
- 412 Strachan, R.A., Alsop, G.I., Ramezani, J., Frazer, R.E., Burns, I.M., Holdsworth, R.E., 2020a.  
413 Patterns of silurian deformation and magmatism during sinistral oblique convergence, northern  
414 scottish caledonides. *J. Geol. Soc. London.* 177, 893–910. <https://doi.org/10.1144/jgs2020-039>
- 415 Strachan, R.A., Holdsworth, R.E., Krabbendam, M., Alsop, G.I., House, M., Rd, W.M., Andrews,  
416 S., 2010. The Moine Supergroup of NW Scotland : insights into the analysis of polyorogenic  
417 supracrustal sequences. *Geol. Soc. London, Spec. Publ.*
- 418 Strachan, R.A., Johnson, T.E., Kirkland, C.L., Kinny, P.D., Kusky, T., 2020b. A Baltic heritage in  
419 Scotland: Basement terrane transfer during the Grenvillian orogeny. *Geology* 48, 1094–1098.  
420 <https://doi.org/10.1130/G47615.1>
- 421 Weller, O.M., 2017. Record of modern-style plate tectonics in the.  
422 <https://doi.org/10.1038/NGEO2904>

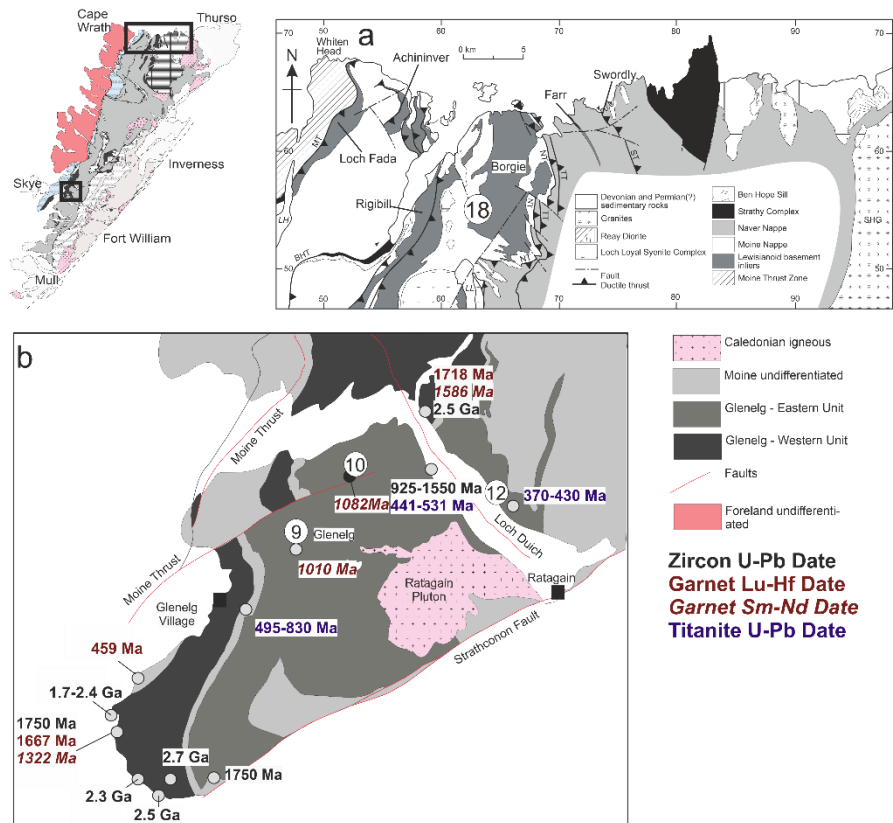
## 423 **7.1 Acknowledgements**

424 The authors would like to thank NERC for funding Bird's PhD during which many of these  
425 analyses was undertaken.



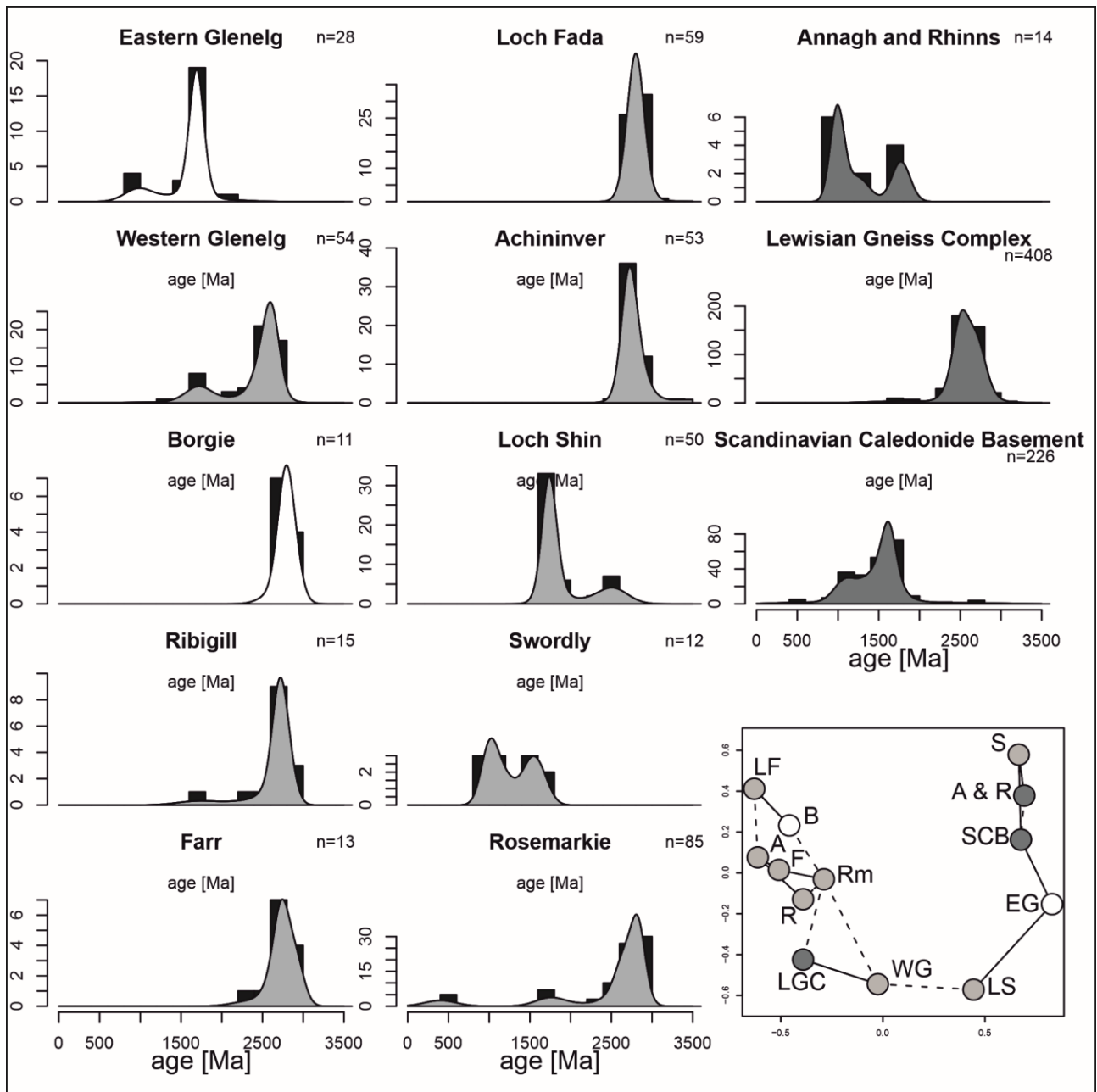
426

427 *Figure 1 Schematic plate reconstruction of the amalgamation of Rodina from 1.7 G.a. to 1.1 G.a. based on the reconstructions of, Li*  
 428 *et al. 2008, Perhsson et al 2016, Cawood et al. 2016 and Cawood & Pisarevsky 2017. Laur = laurentia, S= Scotland, S China =*  
 429 *South China Craton, Sib = Siberian craton, Balt = Baltica, R. Plata = Rio de la Plata craton, G = Grenville orogeny, SN = Sven-*  
 430 *norwegian Orogeny. dark blue with red trim = subduction (red teeth indicate hanging-wall side), Double ended red arrows = ocean*  
 431 *spreading. Red/orange shading = ~1.1G.a. orogenesis.*



432

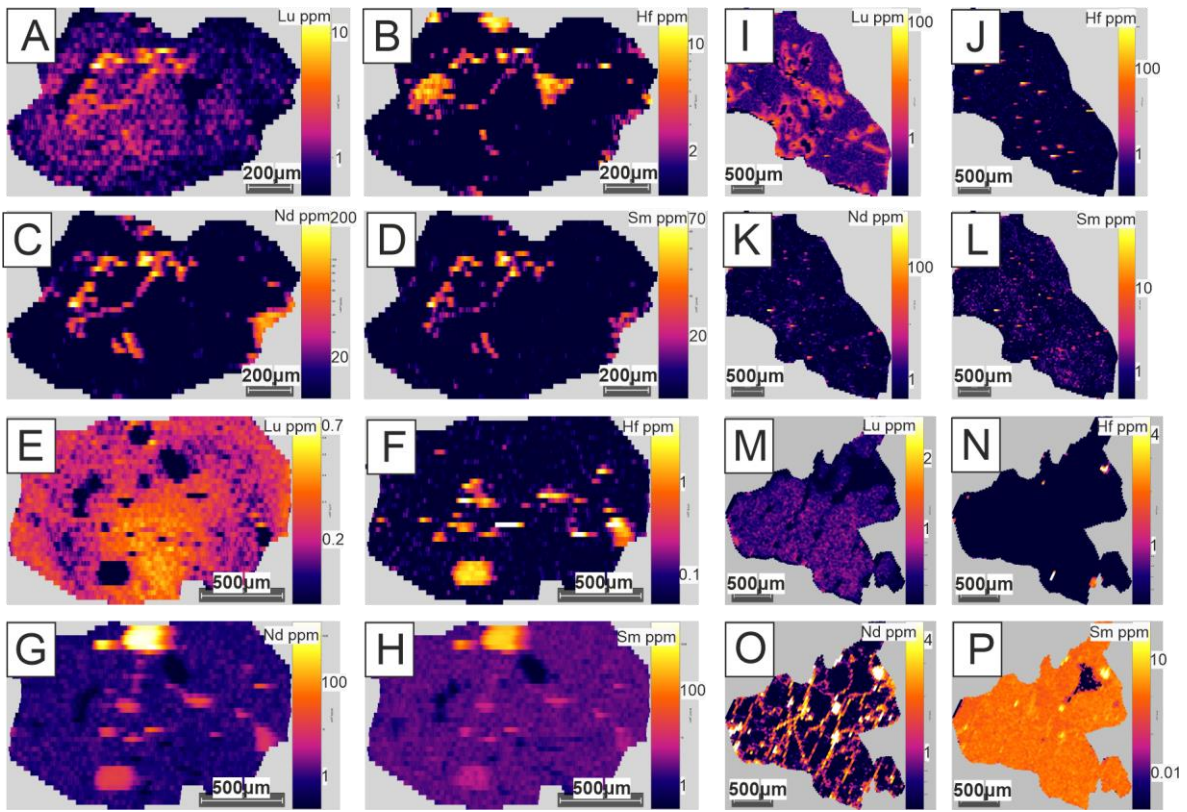
433 *Figure 2 Simplified map of the Northern Highlands, Scotland and study areas. Fig. 2a shows the geology of Northern Sutherland and*  
 434 *the location of the Borgie and other inliers mentioned within the text. Fig. 2b shows the geology of the Glenelg region and the*  
 435 *locations of samples with published data and locations of the samples within this study.*



436

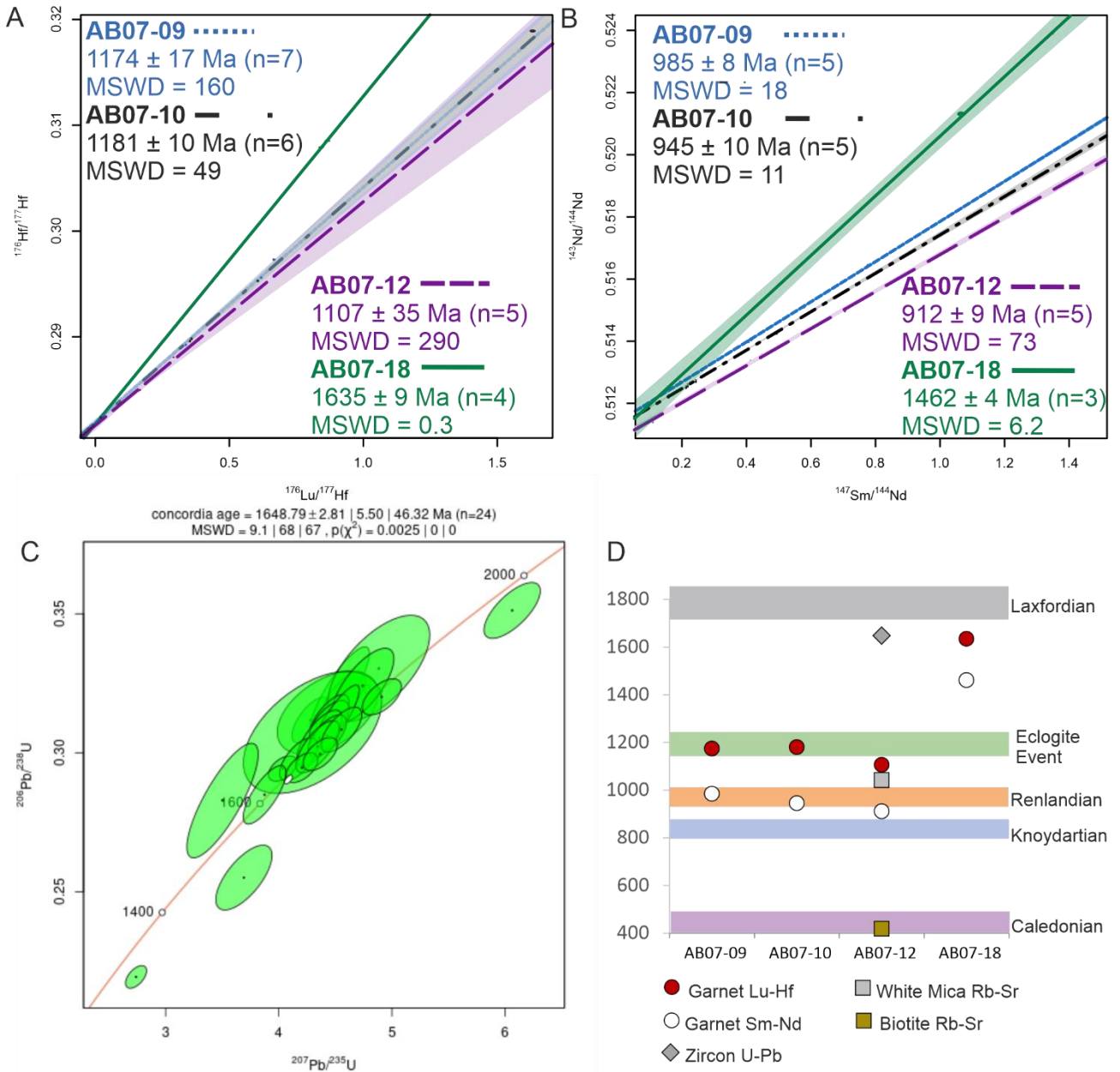
437 *Figure 3 Zircon U-Pb dates for the inliers from Friend et al., 2008; Strachan et al., 2020a; Storey et al., 2010; Brewer et al., 2003;*  
 438 *Mendum and Noble, 2010 . The dates from the Lewisian Gneiss Complex are only from mainland Scotland and are from Baker et al.,*  
 439 *2019; Corfu et al., 1994; Crowley et al., 2015; Davies and Heaman, 2014; Fischer et al., 2021; Love et al., 2004. Irish dates are*  
 440 *from Daly, 1996, 1991. Scandinavian dates are from Bergh et al., 2015; Slagstad and Kirkland, 2017. Only dates less than 15%*  
 441 *discordant have been included. A MDS for these regions using these zircon U-Pb dates is also included; LF – Loch Fada; B –*  
 442 *Borgie; A – Achiniver; F – Farr; Rm – Rosemarkie; R – Ribigill; LGC – Lewisian Gneiss Complex; WG – Western Glenelg; LS –*  
 443 *Loch Shin; EG – Eastern Glenelg; SCB – Scandinavian Caledonide Basement; A & R – Annagh and Rhinns; S – Swordly. All plots*  
 444 *were made using IsoplotR (Vermeesch 2018).*





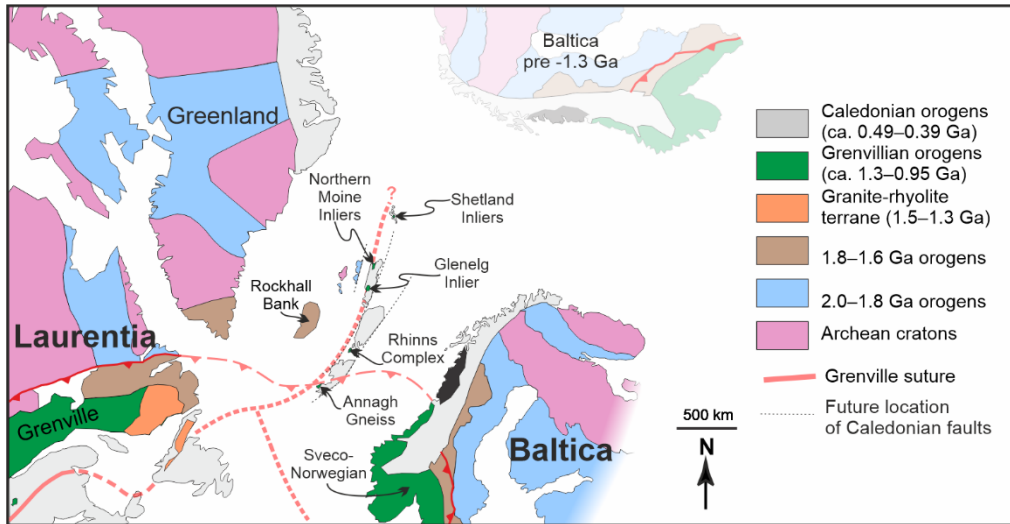
446  
447

Figure 4 LA ICPMS elemental maps of garnets from all samples. A to D are from AB07-09; E to H are from AB07-10; I to L are from AB07-12 and M to P are from AB07-18.



448  
449  
450

Figure 5 A – garnet Lu-Hf data; B - garnet Sm-Nd data; C - zircon U-Pb dates; D - summary plot relating new dates to known orogenic episode.



452 *Figure 6 Distribution of orogenic events on the north Atlantic region as distributed at the end of the Grenville orogeny (modified*  
453 *from Cawood et al 2010) with the position of Baltica prior to the Grenville orogeny also shown (semi-transparent). Location of NHT*  
454 *inliers indicates the revised northern extent of Grenville orogenesis.*

### 455 8.1 Supplementary Data 1

## 456 Eclogites and basement terrane tectonics in the northern arm of the 457 Grenville orogen, NW Scotland

458 A. Bird<sup>1</sup>, M. Thirlwall<sup>2</sup>, R.A. Strachan<sup>3</sup>, I.L. Millar<sup>4</sup>, E.D. Dempsey<sup>1</sup>, K. Hardman<sup>1</sup>

459 1. Department of Geography, Geology and Environment, University of Hull, Cottingham Road,  
460 Hull, HU6 7RX

461 2. Department of Earth Sciences, Royal Holloway University of London, Egham, Surrey, TW20  
462 0EX

463 3. School of the Environment, Geography and Geosciences, University of Portsmouth, Burnaby Rd,  
464 Portsmouth, PO1 3QL.

465 4. Geochronology and Tracers Facility, British Geological Survey, Keyworth, Nottinghamshire,  
466 NG12 5GG

### 467 SUPPLEMENTARY DATA

#### 468 Trace Element LA ICPMS Analyses – University of Hull

##### Laboratory and Sample Preparation

Laboratory name	Geography, Geology and Environment, University of Hull
Sample type/mineral	Metamorphic thick sections
Sample preparation	Polished sections

Imaging Thin Section photos and scans

**Laser ablation system**

Make, Model and type Applied Spectra, RESOLUTION-SE 193nm

Ablation cell and volume Laurin Technic S155 two volumn cell

Laser wavelength 193 nm

Pulse width (ns) 5 ns

Fluence (J cm<sup>-2</sup>) 2.5 J sm<sup>-2</sup>

Repition rate (Hz) 10 Hz

Ablation duration (s) 30s

Spot diameter 30 microns

Sample mode/pattern Raster - Scan Speed 0.002cm/s

Carrier gas He + N2 in the cell, Ar carrier gas to torch

**ICP-MS Instrument**

Make, Model and type Agilent 8800

Sample introduction Ablation aerosol mixed with Ar and sent to ICP-MS

RF power (w) 1170 W

Nebuliser gas flow Ar 0.90 l min<sup>-1</sup>

Detection system Electron multiplier in counts per second mode

Masses measured Mg25, Si29, P31, K39, Ca43, Ti47, Cr52, Fe56, Rb85, Sr88, Y89, Zr90, Ce140, Nd146, Sm146, Eu153, Gd157, Dy163, Yb172, Lu175, Hf178, Pb206, Pb207, U235, U238

Integration time 56 = 0.0005, 90 = 0.002, 89 = 0.003, 25, 31, 39, 29 = 0.004, 88 = 0.005, 85, 43 = 0.006, 52 = 0.008, 147 = 0.015, 235, 238, 206, 178, 208, 47, 207 = 0.02, 140 = 0.04, 175, 153, 157, 163, 172 = 0.05,

**Data Processing**

Calibration strategy Si content used as normalisation channel. 610 and 612 used as secondaries/validation

Reference Material Information NIST610 and NIST612

Data processing package Iolite v4, Cellspace, Semi-Quant (Woodhead et al., 2007; Paton et al., 2011; Paul et al., 2012)

Common Pb correction No common Pb correction applied to this data

469

470 **LA ICPMS Elemental Maps**

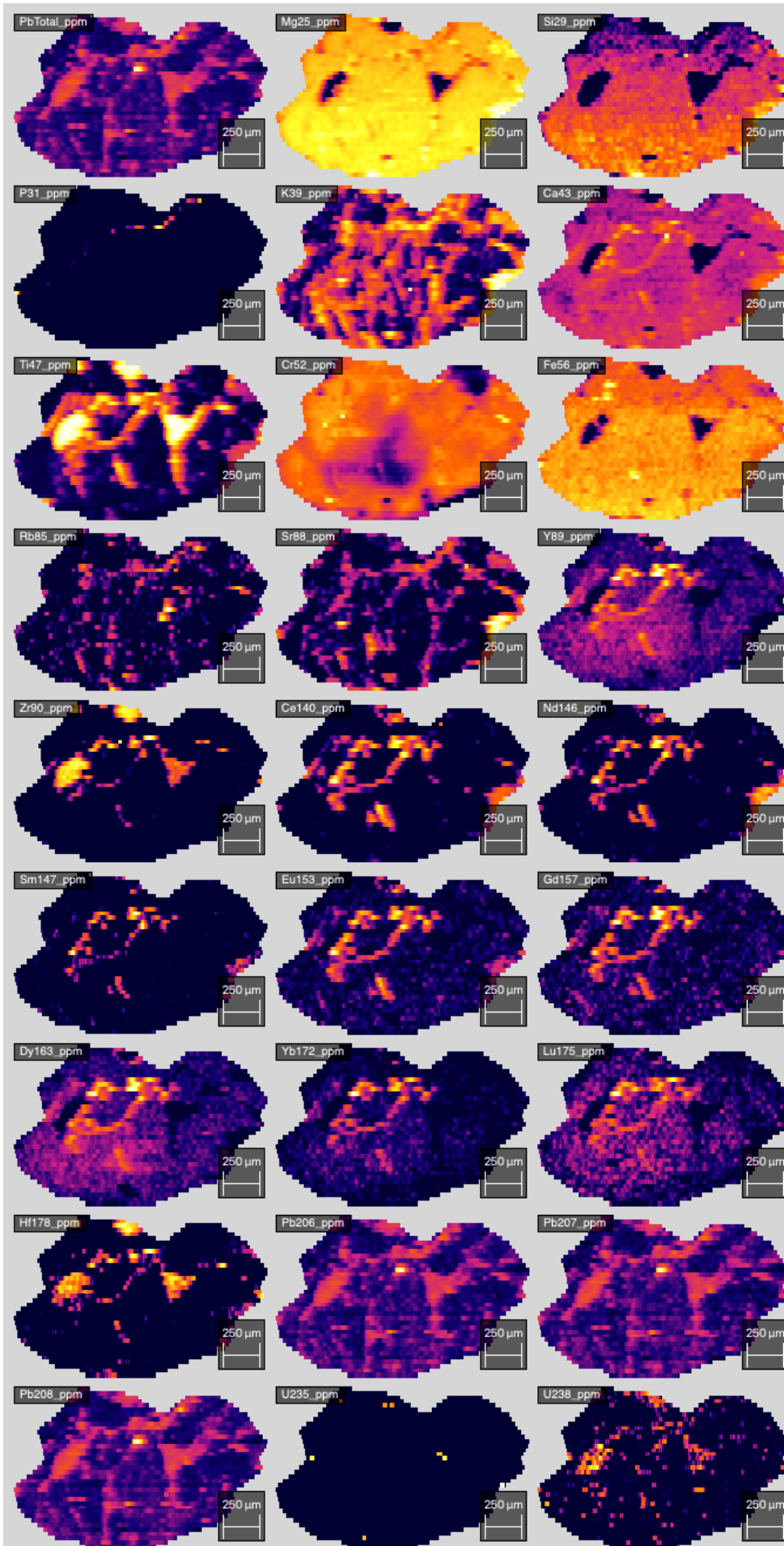
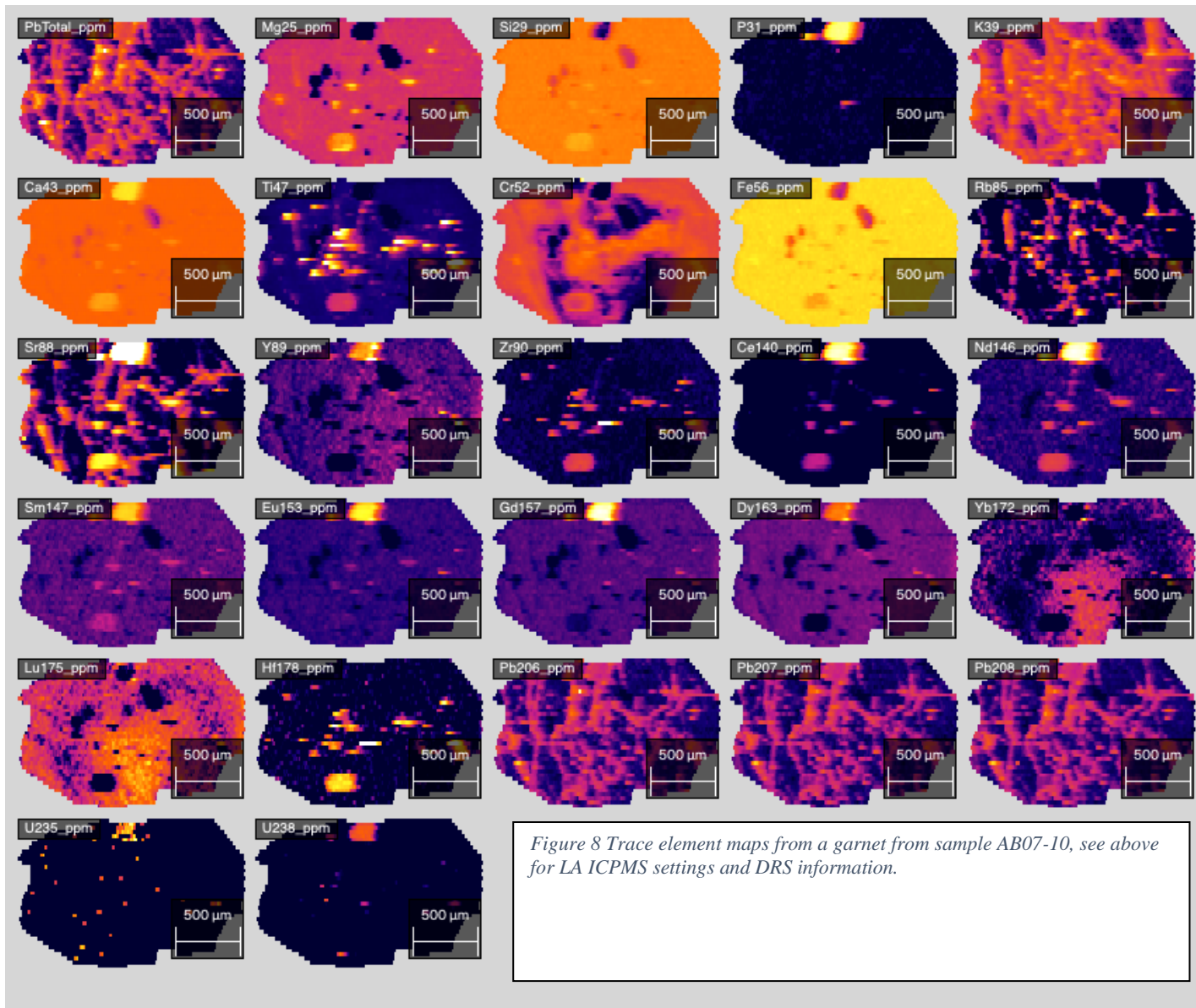
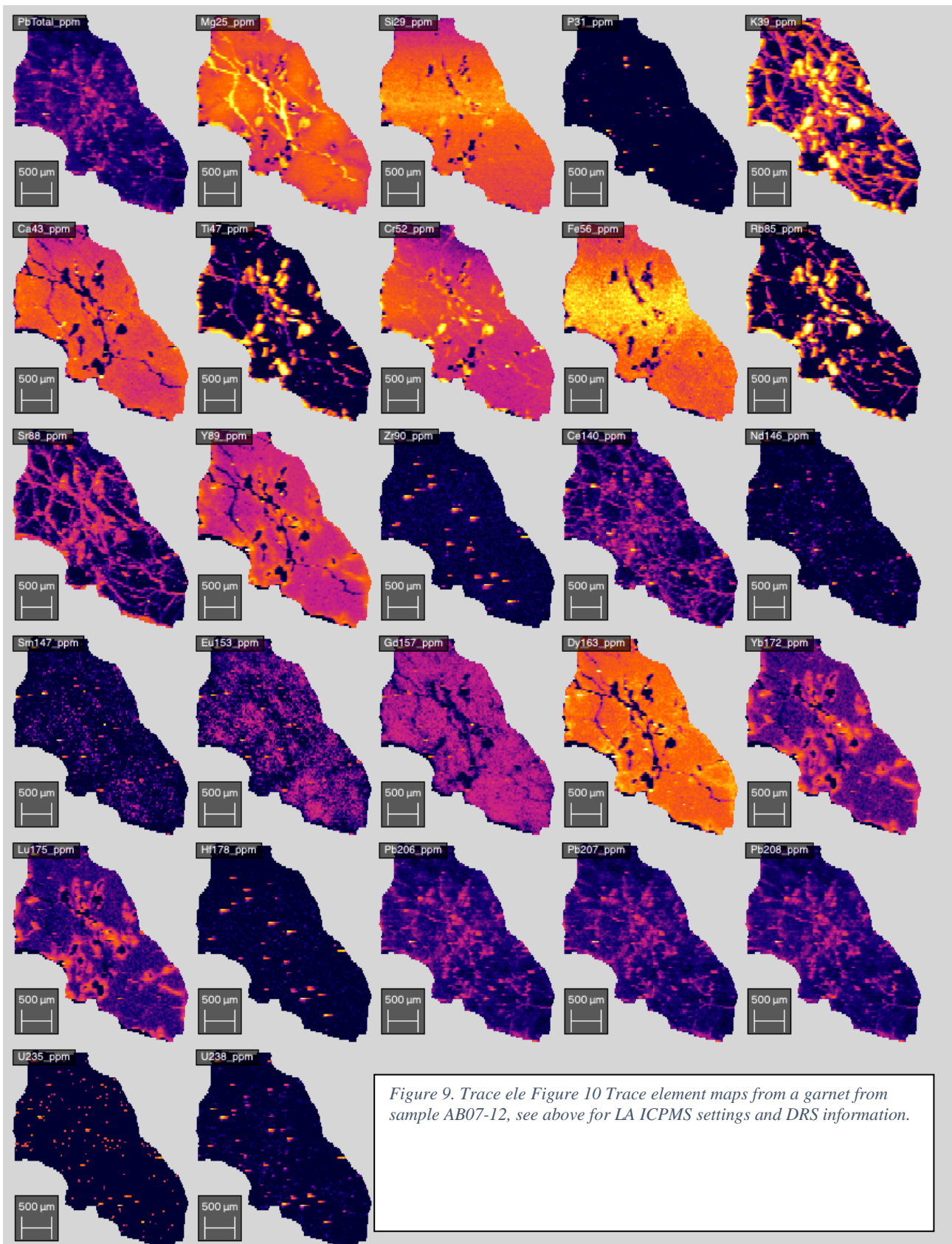


Figure 7. Trace element maps from a garnet from sample AB07-09, see above for LA ICPMS settings and DRS information

472



473



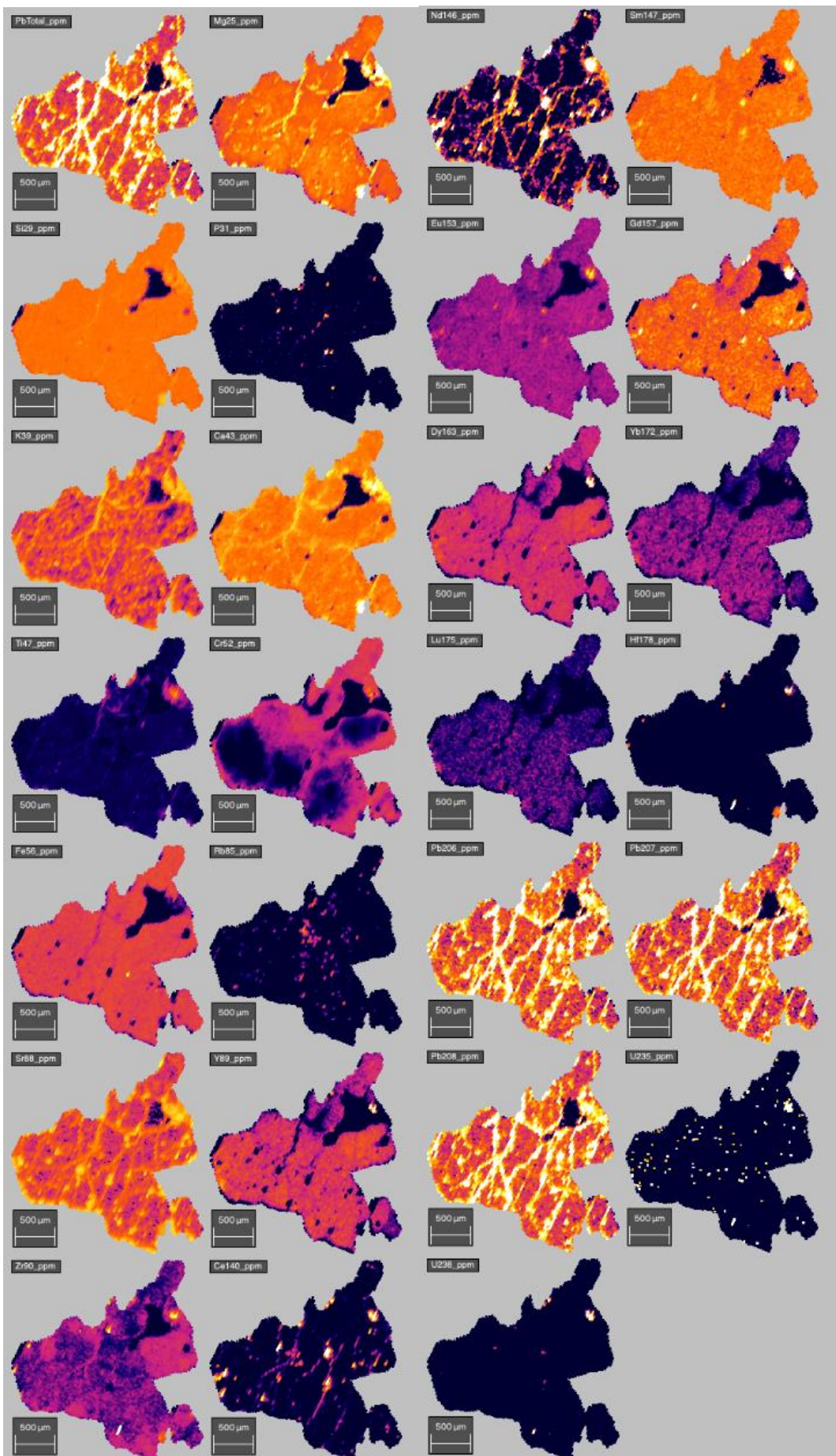


Figure 11. Trace element maps from a garnet from sample AB07-18, see above for LA ICPMS settings and DRS information



476 **LA ICPMS U-Pb Analyses – British Geological Survey****Laboratory and Sample Preparation**

Laboratory name	Geochronology & Tracers Facility, BGS, Keyworth, UK
Sample type/mineral	Zircon grains
Sample preparation	Conventional mineral separation, 1-inch resin mount, 1µm polish to finish
Imaging	Photos

**Laser ablation system**

Make, Model and type	ESI/New Wave Research, UP193SS
Ablation cell and volume	NIGL low volume cell, with low effective volume (ca. 3-4 cm <sup>3</sup> ), washout time ca. 1 sec
Laser wavelength	193 nm
Pulse width (ns)	3-4 ns
Fluence (J cm <sup>-2</sup> )	2.6 J cm <sup>2</sup>
Repetition rate (Hz)	10 Hz
Ablation duration (s)	30 s
Spot diameter	35 microns
Sample mode/pattern	Static spot ablation
Carrier gas	0.6 l/min

**ICP-MS Instrument**

Make, Model and type	Nu Instruments Attom SC-ICP-MS
Sample introduction	Free air aspiration of desolvator
RF power (w)	1300W
Nebuliser gas flow	0.70 l min <sup>-1</sup>
Detection system	Discrete dynode MassCom ion counter
Masses measured	Pb204, Pb206, Pb207, Pb208, Th232, U235, U238
Integration time per peak	ca. 200 ms
Integration time/reading	Ca.1 sec
Sensitivity	Not determined
IC Dead time (ns)	15 ns

**Data Processing**

Gas blank	>30 second on-peak zero subtracted
Calibration strategy	91500 used as primary reference material and GJ1 and Plesovic used as secondaries/validation
Reference Material Information	91500 (Wiedenbeck et al. 1995) Plešovice (Sláma et al. 2008), GJ-1 (Horstwood et al. 2016).
Data processing package	Nu Instruments TRA acquisition software, In-house spreadsheet.
Common Pb correction	No common Pb correction applied to this data

477

478 **Lu-Hf, Sm-Nd and Rb-Sr analyses – RHUL**

479 Samples were crushed in a steel jaw-crusher to chips of < 1cm<sup>3</sup>. A fraction of this crushed material  
 480 was saved for whole rock analysis, which was powdered in a tungsten carbide TEMA mill ready for  
 481 XRF and isotopic analysis. The X-ray fluorescence (XRF) analyses were also undertaken at Royal

482 Holloway using the methods described by Thirlwall et al. (2000). This remaining material was sieved  
483 to different grain sizes, washed repeatedly in de-ionised water, and magnetically separated using a  
484 Frantz isodynamic separator. Garnets and other mineral fractions were handpicked under a binocular  
485 microscope from the 250-500 $\mu$ m magnetic fraction, taking care to pick only grains that were visibly  
486 inclusion-free. Mica fractions were then ground in an agate pestle and mortar under methanol, washed  
487 in MQ water, and further sieved between 200 and 75 $\mu$ m to remove non-mica impurities, then picked  
488 under a binocular microscope from the <250 $\mu$ m fraction. The garnet fractions underwent a moderate  
489 leaching procedure using sulfuric acid, (Anczkiewicz & Thirlwall 2003; Bird et al 2013; Walker et al  
490 2020), this dissolves phosphate inclusions that can negatively affect Sm-Nd ages.

491 Amounts of mixed  $^{176}\text{Lu}/^{180}\text{Hf}$ ,  $^{149}\text{Sm}/^{150}\text{Nd}$  and  $^{87}\text{Rb}/^{84}\text{Sr}$  spike spikes for mineral separates  
492 and whole-rocks were estimated using concentrations of these elements, and of analogues such as Y  
493 and Zr, from LA-ICPMS and XRF respectively. Leaching, spiking, dissolution, and chemical  
494 separation procedures were those of Anczkiewicz & Thirlwall (2003), Bird et al. (2013), Walker et  
495 al (2016; 2020) with concentrations and isotopic data being determined on the same aliquot.

496 A HF-HNO<sub>3</sub> digestion procedure was utilized for all fractions in sealed beakers on a hotplate,  
497 followed by a dissolution in 6M HCl for the garnet fractions. This minimizes dissolution of refractory  
498 zircon inclusions, which can worsen the precision of Lu-Hf ages, as they have very high Hf  
499 concentrations. Further, detrital zircons in metasediments can be much older than the surrounding  
500 garnets, which may artificially skew the age of any mixtures of garnets and zircons (Anczkiewicz et  
501 al. 2004).

502 For the whole-rock fractions analysed for Lu-Hf, we treated one fraction in the same manner  
503 as the garnets (table-top dissolution using HF-HNO<sub>3</sub>), and a second whole-rock powder fraction was  
504 fused for one hour at 1100°C in Pt-Au crucibles in a 1:3 ratio with lithium tetraborate flux. Glass  
505 fragments were then spiked and subjected to the normal Lu-Hf dissolution and chemical separation.  
506 The samples were first passed through AG50W-X8 cation resin to separate high field strength  
507 elements (HFSE), light rare earth elements (LREE) and heavy rare earth elements (HREE) fractions.  
508 The HFSE fraction required a second pass through these columns to minimise the HREE that may be  
509 in the fraction. The fractions were individually passed through Eichrom LN resin to separate  
510 respectively Hf, Sm and Nd, and Lu. Total procedure blanks were typically 24pg for Hf and 23pg  
511 for Nd. Sr was separated using Eichrom Sr-spec resin, and Rb was separated from K using 0.5M  
512 HNO<sub>3</sub> on Bio-rad AG50W-X8 cation exchange resin.

513 Lu, Hf, Sm Nd and Rb isotopic analyses were undertaken on the GV Instruments IsoProbe  
514 MC-ICPMS at RHUL using methods outlined in Thirlwall & Anczkiewicz (2004), Bird et al (2013)  
515 and Walker et al 2016; 2020.

516 During the course of the study the Hf standard JMC475 analysed on the RHUL IsoProbe  
517 yielded an average (static)  $^{176}\text{Hf}/^{177}\text{Hf}$  of  $0.282182\pm 12$  and  $^{180}\text{Hf}/^{177}\text{Hf}$  of  $1.88683\pm 17$  (2sd, n=36),  
518 with no significant change with time. All sample data were corrected to the accepted JMC475  
519  $^{176}\text{Hf}/^{177}\text{Hf}$  value of 0.282165 (Scherer et al. 2000).

520 In contrast to Hf, Nd standard isotope ratios can vary significantly between analytical sessions  
521 (Thirlwall and Anczkiewicz 2004), although the effect of this on ages was minimized by analyzing  
522 all fractions relating to a sample during one analytical session. The Aldrich Nd and mixed Ce-Nd  
523 standard solutions yielded  $^{142}\text{Nd}/^{144}\text{Nd}$  of  $1.141461\pm 239$  and a slope corrected (see Thirlwall &  
524 Anczkiewicz 2004)  $^{143}\text{Nd}/^{144}\text{Nd}$  of  $0.511408\pm 14$  (2sd, n=97). The uncertainty on the  $^{176}\text{Lu}/^{177}\text{Hf}$  ratio  
525 is less than 0.3% and assumed to be 0.3% in age calculations. The uncertainty on the  $^{147}\text{Sm}/^{144}\text{Nd}$  is  
526 less than 0.1% and assumed to be 0.1% in age calculations.

527 Correction of mass fractionation of Rb used methods described in Walker et al 2016, this technique  
528 allows for the correction of the mass fractionation of Rb using Zr, leading to higher precision  
529 compared with conventional TIMS analysis, where mass fractionation correction possibilities are  
530 limited (Halliday et al 1998; Waight *et al.* 2002). Uncertainties on Rb/Sr ratios were monitored  
531 using the method described in Walker et al, 2016, modified from Waight *et al.* (2002), where the  
532 normalizing Zr ratios ( $^{92}\text{Zr}/^{90}\text{Zr}$  and  $^{91}\text{Zr}/^{90}\text{Zr}$ ) was used to correct for Rb mass fractionation are  
533 determined daily using the Sr standard SRM987 admixed with Zr (see Charlier *et al.* 2006). The Rb  
534 standard SRM984 was analysed at least every four samples during analytical sessions ( $n = 31$  for  
535 the duration of this study), to test the accuracy and precision of this technique.

536 Analysed for Sr isotopes by TIMS were undertaken on a VG354 system. Isotope ratios and  
537 concentrations were determined using a multidynamic method modified from Thirlwall (1991). The  
538 accuracy and reproducibility of Sr isotope data were monitored using the external standard  
539 SRM987. During the course of this study,  $^{87}\text{Sr}/^{86}\text{Sr}$  of SRM987 was  $0.710256 \pm 19$  2SD. Total  
540 procedural blanks for Sr were typically less than 0.2% (0.5 ng) of the analyte mass, and hence a  
541 blank correction has no significant effect on ages presented. The  $^{87}\text{Rb}/^{86}\text{Sr}$  uncertainty used in age  
542 calculations was taken as 0.3% ( $2\sigma$ ), although this is likely to be an overestimate.

543 Isochron ages and uncertainties were calculated using IsoplotR (Vermeesch, 2018), using the  
544 decay constants of  $1.865 \times 10^{-11} \text{ a}^{-1}$  for  $^{176}\text{Lu}$  (Scherer et al. 2001),  $6.524 \times 10^{-12} \text{ a}^{-1}$  for  $^{147}\text{Sm}$  (Villa

545 et al 2020), and  $1.3792 \times 10^{-11} \text{a}^{-1}$  for  $^{87}\text{Rb}$  (Villa *et al.* 2015). All isotope data and age uncertainties  
546 are quoted at the 2-sigma level and uncertainties from Nd and Hf standards have been propagated  
547 into the date calculations.

548 REFERENCES CITED

- 549 Anczkiewicz, R., & Thirlwall, M. F. (2003). Improving precision of Sm-Nd garnet dating by  
550 H<sub>2</sub>SO<sub>4</sub> leaching: a simple 815 solution to the phosphate inclusion problem. *Journal of the*  
551 *Geological Society, London*, 220, 83–91.
- 552 Anczkiewicz, R., Platt, J. P., Thirlwall, M. F., & Wakabayashi, J. (2004). Franciscan subduction off  
553 to a slow start: 817 evidence from high-precision Lu–Hf garnet ages on high grade-blocks.  
554 *Earth and Planetary Science Letters*, 225(1–2), 147–161.  
555 <https://doi.org/10.1016/j.epsl.2004.06.003>
- 556 Baxter, E. F., Ague, J. J., & Depaolo, D. J. 2000. Prograde temperature – time evolution in the  
557 Barrovian type – 825 locality constrained by Sm / Nd garnet ages from Glen Clova, Scotland.  
558 *Journal of the Geological Society, London*, 159(1985), 71–82.
- 559 Bird, A.F., Thirlwall, M.F., Strachan, R.A., Manning, C.J., Holloway, R., Oex, E.T.W., 2013. Lu –  
560 Hf and Sm – Nd dating of metamorphic garnet : evidence for multiple accretion events during  
561 the Caledonian orogeny in Scotland 170, 301–317. doi:10.1144/jgs2012-083.Lu
- 562 B.L.A. Charlier, C. Ginibre, D. Morgan, G.M. Nowell, D.G. Pearson, J.P. Davidson, C.J. Ottley.  
563 2006. Methods for the microsampling and high-precision analysis of strontium and rubidium  
564 isotopes at single crystal scale for petrological and geochronological applications, *Chemical*  
565 *Geology*, Volume 232, Issues 3–4, 2, Pages 114-133
- 566 Alex N. Halliday, Der-Chuen Lee, John N. Christensen, Mark Rehkämper, Wen Yi, Xiaozhong  
567 Luo, Chris M. Hall, Chris J. Ballentine, Thomas Pettke, Claudine Stirling. 1998. Applications  
568 of multiple collector-ICPMS to cosmochemistry, geochemistry, and paleoceanography.  
569 *Geochimica et Cosmochimica Acta*, 62, 919–940.
- 570 Scherer, E.E., Cameron, K.L., Blichert-Toft, J., 2000. Lu – Hf garnet geochronology : Closure  
571 temperature relative to the Sm – Nd system and the effects of trace mineral inclusions.  
572 *Geochim. Cosmochim. Acta* 64, 3413–3432.
- 573 Thirlwall, M.F. 1991. Long-term reproducibility of multicollector Sr and Nd isotope ratio analysis.  
574 *Chemical Geology*, 94, 85–104.

- 575 Thirlwall, M. F., & Anczkiewicz, R. 2004. Multidynamic isotope ratio analysis using MC–ICP–MS  
576 and the causes of secular drift in Hf, Nd and Pb isotope ratios. *International Journal of Mass*  
577 *Spectrometry*, 235(1), 59–81. <https://doi.org/10.1016/j.ijms.2004.04.002>
- 578 Vermeesch, P., 2018, IsoplotR: a free and open toolbox for geochronology. *Geoscience Frontiers*,  
579 v.9, p.1479-1493, doi: 10.1016/j.gsf.2018.04.001
- 580 Villa, I.M., De Bièvre, P., Holden, N.E. & Renne, P.R. 2015. IUPAC–IUGS recommendation on  
581 the half life of <sup>87</sup>Rb. *Geochimica et Cosmochimica Acta*, 164, 382–385.
- 582 I.M. Villa, N.E. Holden, A. Possolo, R.B. Ickert, B. Hibbert, P.R. Renne. 2020. IUPAC-IUGS  
583 recommendation on the half-lives of <sup>147</sup>Sm and <sup>146</sup>Sm. *Geochimica et Cosmochimica Acta*,  
584 285, 70-77.
- 585 Walker, S., Thirlwall, M.F., Strachan, R.A., Bird, A.F., 2016. Evidence from Rb-Sr mineral ages  
586 for multiple orogenic events in the caledonides of Shetland, Scotland. *J. Geol. Soc. London*.  
587 173. doi:10.1144/jgs2015-034
- 588 Waight, T., Baker, J. & Willigers, B. 2002. Rb isotope dilution analyses by MC-ICPMS using Zr to  
589 correct for mass fractionation: Towards improved Rb–Sr geochronology? *Chemical Geology*,  
590 186, 99–116.
- 591 Woodhead, J., Hellstrom, J., Hergt, J., Greig, A. & Maas, R (2007) Isotopic and elemental imaging  
592 of geological materials by laser ablation Inductively Coupled Plasma mass spectrometry. *Journal of*  
593 *Geostandards and Geoanalytical Research*, 31, p. 331-343.
- 594 Paton, C., Hellstrom, J., Paul, B., Woodhead, J. and Hergt, J. (2011) Iolite: Freeware for the  
595 visualisation and processing of mass spectrometric data. *Journal of Analytical Atomic*  
596 *Spectrometry*. doi:10.1039/c1ja10172b.
- 597 Paul, B., Paton, C., Norris, A., Woodhead, J., Hellstrom, J., Hergt, J., and Greig, A. (2012)  
598 CellSpace: A module for creating spatially registered laser ablation images within the Iolite  
599 freeware environment. *Journal of Analytical Atomic Spectrometry*, v. 27, no. 4, p. 700, doi:  
600 10.1039/c2ja10383d.
- 601